Causality of the Drought in the Southwestern United States Based on Observations

FENG ZHANG

Key Laboratory of Meteorological Disaster, Ministry of Education, Nanjing University of Information Science and Technology, Nanjing, China, and Center for Atmospheric and Oceanic Studies, Graduate School of Science, Tohoku University, Sendai, Japan

YADONG LEI AND QIU-RUN YU

Key Laboratory of Meteorological Disaster, Ministry of Education, Nanjing University of Information Science and Technology, Nanjing, China

KLAUS FRAEDRICH

Max Planck Institute for Meteorology, Hamburg, Germany

HIRONOBU IWABUCHI

Center for Atmospheric and Oceanic Studies, Graduate School of Science, Tohoku University, Sendai, Japan

(Manuscript received 16 August 2016, in final form 22 February 2017)

ABSTRACT

Slow feature analysis is used to extract driving forces from the monthly mean anomaly time series of the precipitation in the southwestern United States (1895–2015). Four major spectral scales pass the 95% confidence test after wavelet analysis of the derived driving forces. Further harmonic analysis indicates that only two fundamental frequencies are dominant in the spectral domain. The frequencies represent the influence of the Pacific decadal oscillation (PDO) and solar activity on the precipitation from the southwestern United States. In addition, solar activity has exerted a greater effect than the PDO on the precipitation in the southwestern United States over the past 120 years. By comparing the trend of droughts with the two fundamental frequencies, it is found that both the droughts in the 1900s and in the twenty-first century were affected by the PDO and solar activity, whereas the droughts from the 1950s to the 1970s were mainly affected by solar activity.

1. Introduction

Instrumental records and paleoclimatic evidence show that the southwestern United States has suffered from several severe droughts in recent years (Cook et al. 2011, 2013, 2014, 2016; Cook et al. 1999, 2004, 2007, 2010; Woodhouse et al. 2010; Touchan et al. 2011; Fawcett et al. 2011; Oglesby et al. 2012; Chylek et al. 2014). Therefore, studies of the causes of the droughts are important. Previous studies analyzed the reasons for droughts in the southwestern United States by using statistical methods (correlation and regression analyses) and numerical modeling experiments (Cook et al. 2011, 2013, 2016). Recent research suggests that these droughts are related to El Niño–Southern Oscillation (Douglas and Englehart 1981; Kiladis and Diaz 1989; Touchan et al. 2011), the Pacific decadal oscillation (PDO; Mantua et al. 1997; Gershunov and Barnett 1998; Oglesby et al. 2012; Chylek et al. 2014), the Atlantic multidecadal oscillation (Enfield et al. 2001; McCabe et al. 2004; Curtis 2008; Feng et al. 2011; Chylek et al. 2014), and land surface forcing (Cook et al. 2013, 2014). However, uncertainties in the physical, chemical, and biological processes remain in the model simulations, making them unable to describe the real world sufficiently. For statistical methods, correlation does not mean causality, and correlation analysis alone cannot confirm whether causality exists. However, it is

noteworthy that, in recent years, physics and economics studies have increasingly focused on the development of techniques to reconstruct driving forces based on non-linear and nonstationary dynamics (Eckmann et al. 1987; Casdagli 1997; Verdes et al. 2001; Wiskott 2003). 1) The earliest method to estimate driving forces for systems with unknown dynamics dates back to recurrence plots (Eckmann et al. 1987; Casdagli 1997). Although partial information about driving forces can be obtained, their character can only be depicted approximately by re-currence plots. 2) Another relatively accurate method is based on cross-prediction errors from two intervals of a time series (Verdes et al. 2001). The prediction error is calculated by a radial basis function network for pre-dicting the overlapping intervals of the time series. However, the performance of the technique depends heavily on the number of samples that do not overlap between two consecutive intervals. Thus, it cannot be applied to steady or relatively stationary time series. 3) To solve the deficiencies of the methods, Wiskott (2003) developed slow feature analysis (SFA), which originated in the field of theoretical neurobiology, to evaluate the driving forces of a nonstationary time series. Konen (2009) modified SFA based on singular value de-composition. The method works for slowly and rarely varying driving forces and is fairly robust to noise.

These three methods reconstruct driving forces di-rectly from the observation data, and they do not need a mathematical model to describe unknown dynamical systems. Therefore, the results of these methods could avoid discrepancies owing to the uncertainty of models. Recently, Yang et al. (2016) successfully applied SFA to analyze the causality of global warming. Wang et al. (2016) derived the driving force from ozone data by using SFA. Their results show that SFA is a powerful tool for analyzing causality within the climate system. However, to the best of our knowledge, the cause of the change in precipitation has not been investigated by SFA.

In this paper, the driving forces of the precipitation time series from January 1895 to December 2015 in the south-western United States are retrieved by SFA. In addition, wavelet analysis is also used for the time-scale structure analysis of the derived driving forces. In section 2, we briefly describe the data source and the principles of SFA. More-over, the accuracy of the SFA algorithm is tested by using idealized experiments. The results are presented in section 3. Finally, the results are discussed in section 4.

2. Methodology and data

a. Methodology

In this study, the SFA method is used to extract driving forces from a quickly varying time series. The details of
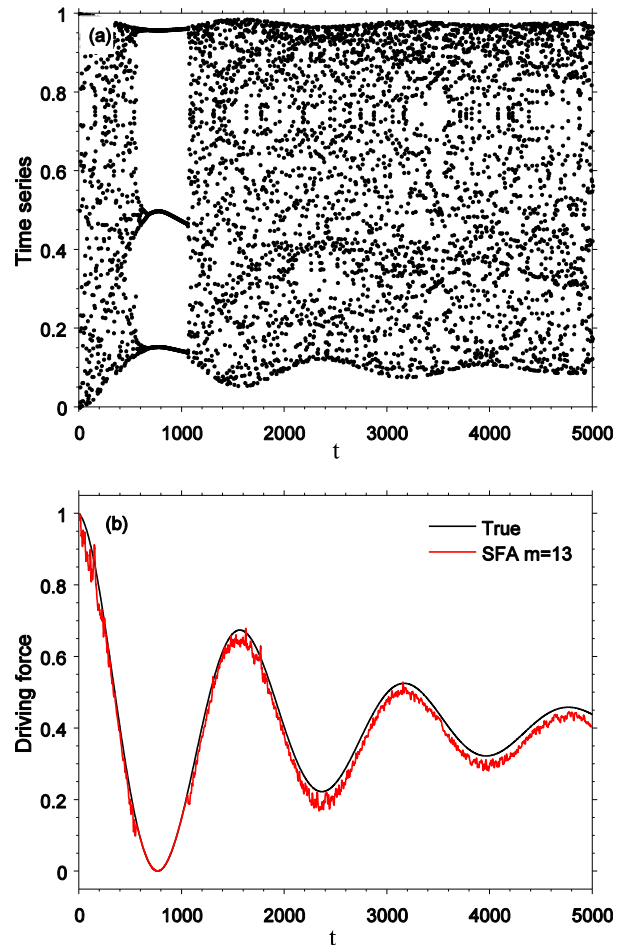

FIG. 1. (a) Time series generated by the logistic map; (b) curves of the normalized true and reconstructed driving forces, denoted by black and red lines, respectively.

SFA have been discussed by Wiskott (2003), Konen (2009), Yang et al. (2016), and Wang et al. (2016). A brief description of some of the steps of SFA is given as follows. First, a given time series $\{x(t)\}_{t=t_1,\ldots,t_n}$ is con-sidered, where t is time and n is the length of the time series. Then $\{x(t)\}_{t=t_1,\ldots,t_n}$ is embedded into m-dimensional state space $\mathbf{X}(t) = \{x_1(t), x_2(t), \ldots, x_m(t)\}_{t_1,\ldots,t_N}$, with $N = n - m + 1$. Then, second-order polynomials are used to generate a K-dimensional function state space: $\mathbf{H}(t) = \{x_1(t), \ldots, x_m(t); x_1^2(t), \ldots, x_1(t)x_m(t); \ldots; x_{m-1}^2(t), x_{m-1}(t)x_m(t); x_m^2(t)\}_{t=t_1,\ldots,t_N}$. For simplifica-tion, $\mathbf{H}(t) = \{h_1(t), h_2(t), \ldots, h_K(t)\}_{t=t_1,\ldots,t_N}$ is rewritten as $K = m + m(m + 1)/2$. The term $\mathbf{H}(t)$ is unified to a sphere to construct coordinate components $\mathbf{H}'(t) = \{h'_1(t), h'_2(t), \ldots, h'_K(t)\}_{t=t_1,\ldots,t_N}$ with unit covari-ance $h'_j {h'_j}^{\mathrm{T}} = 1$ and zero mean $\overline{h'_j} = 0$, where $h'_j(t) = [h_j(t) - \overline{h_j}]/S$ and $S = K^{-1}\sqrt{\sum_{j=1}^{K}[h_j(t) - \overline{h}]^2}$. Next, $\mathbf{H}'(t)$ is orthogonalized into $\mathbf{Z}(t) = \{z_1(t), z_2(t), \ldots, z_K(t)\}_{t=t_1,\ldots,t_N}$
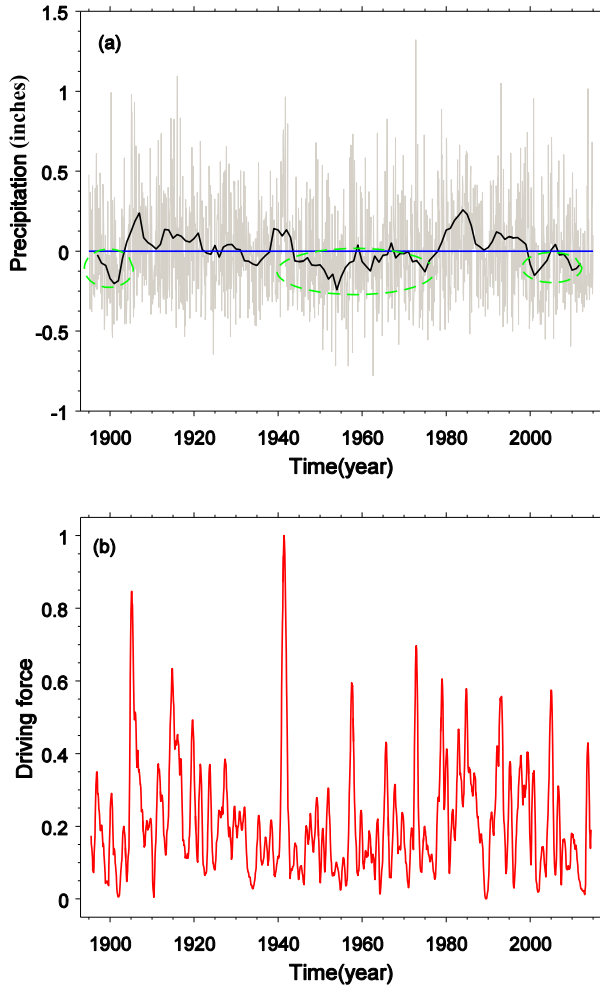
FIG. 2. (a) Monthly precipitation anomaly (in.; 1 in. ≈ 2.54 cm) time series (gray line) with the seasonal cycle removed and 5-yr moving average (black line) in the southwestern United States. (b) Normalized driving force generated by SFA when $m = 13$ (red line).
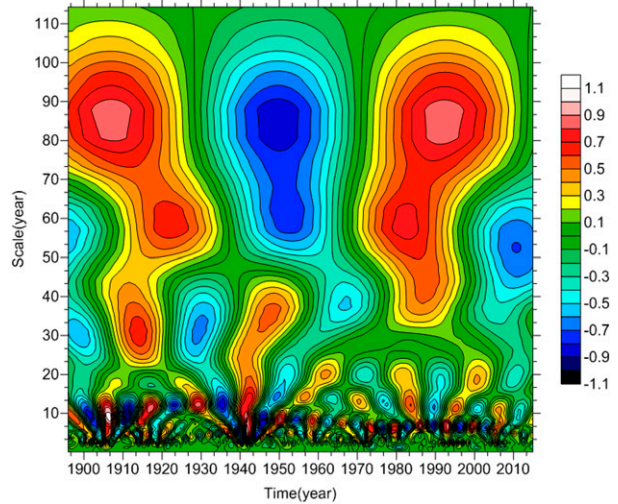

FIG. 3. Real part of the wavelet transform coefficient for the reconstruction of the driving force extracted from the monthly mean precipitation anomaly in the southwestern United States.

by the Schmidt algorithm before calculating the time-derivative $K \times K$ covariance matrix $\mathbf{B} = \dot{\mathbf{Z}}\dot{\mathbf{Z}}^T$ with $\dot{\mathbf{Z}}(t) = \{\dot{z}_1(t), \dot{z}_2(t), \ldots, \dot{z}_K(t)\}_{t=t_1,\ldots t_N}$, where its eigenvalues are $\lambda_1 \leq \lambda_2 \leq \ldots \leq \lambda_K$ and the corresponding eigenvectors are $\mathbf{W}_1, \ldots, \mathbf{W}_K$. Using $\mathbf{W}_1$, the driving force can be written as $y_1(t) = \mathbf{W}_1 \cdot \mathbf{Z}(t)$. In addition, Wiskott (2003) and Konen (2009) show that driving force $y_1(t)$ reconstructed from SFA is robust despite the variation in embedding dimension m.

Next, an experiment with time series s_t from a logistic map is shown, which is a classical theory model, to demonstrate the properties of the SFA algorithm. The time-varying logistic map is $s_{t+1} = u_t s_t (1 - s_t)$, where s_t is the time series and u_t is the driving force. A variation given by $u_t = C \cos(2\pi t/T_1) \exp(-t/T_2) + B$ is considered, where $C = 0.1$, $B = 3.9$, $T_1 = 1600$, and $T_2 = 2000$. In the

experiment, 5000 time series s_t are used (Fig. 1a). The driving force u_t is extracted from s_t by SFA with the embedding dimension $m = 13$. The original and reconstructed forces are normalized; thus, both forces are between 0 and 1. Figure 1b compares the original and reconstructed forces. The correlation coefficient is 0.997 between the original and reconstructed forces, demonstrating that SFA can produce highly accurate results.

b. Data

The data for the precipitation records of the southwestern United States are provided by the National Oceanic and Atmospheric Administration (NOAA)/ National Climatic Data Center (http://www.ncdc.noaa.gov/cag/time-series/us). The data consist of 1440 months covering January 1895–December 2015. For convenience, the southwestern United States is considered as a region composed of Arizona, Colorado, New Mexico, and Utah. Figure 2a shows the monthly mean precipitation anomaly time series (gray line) and its 5-yr moving average (black line). The precipitation in the southwestern United States has experienced several major fluctuations in the past 120 years with major droughts in the 1900s, from the 1950s to the 1970s, and at the beginning of the twenty-first century indicated by the green ellipses in Fig. 2a.

3. Results

The driving force extracted from the monthly mean precipitation anomaly in the southwestern United States is presented in Fig. 2b. The red line (Fig. 2b) demonstrates the normalized driving force reconstructed by SFA with
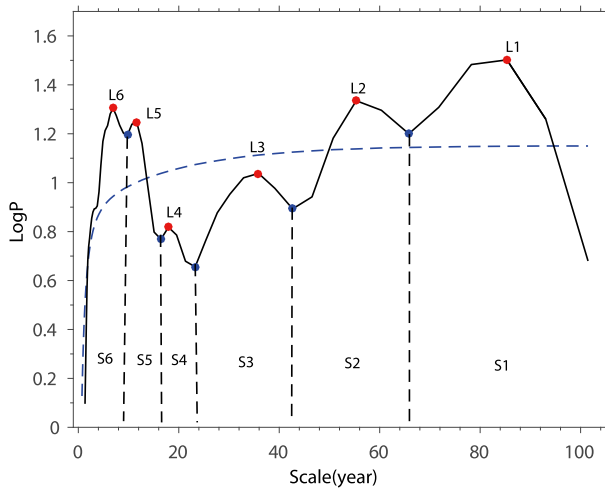
FIG. 4. Time-averaged power spectrum for the reconstruction of the driving force extracted from the monthly mean precipitation anomaly in the southwestern United States. The blue dashed line represents the 95% confidence test. The red (blue) points represent the max (min) values of the time-averaged power spectrum. S1–S6 represent the driving-force spectra.

the embedding dimension $m = 13$, which represents a time resolution of approximately 1 year for the driving force. Several strong peaks in the driving force occur in accordance with the monthly precipitation anomaly. The wavelet analysis approach is used (Gollub and Benson 1980; Zhong and Yang 1986) to investigate the variable characteristics of the driving force. Figure 3 shows the local wavelet power spectrum (Morlet wavelet) of the normalized driving force to reveal the time-scale structure of the driving force, as well as its variations in period and amplitude. The dominating spectral scales are around 7, 11, 18, 36, 55, and 85 yr, which correspond to the maximum energy at each band. As shown in Fig. 4, the driving force mainly consists of six spectral bands, which are denoted as Sk ($k = 1, \ldots, 6$).

Table 1 shows the major parameters of each component, where L_k and f_k ($k = 1, \ldots, 6$) represent the period and frequency of each spectral peak, respectively. Only L_1, L_2, L_5, and L_6 pass the confidence test (95% level), as shown by values exceeding the blue dashed line in Fig. 4. The following results are notable: (i) The significant

periods, L_1, L_2, L_5, and L_6, are 85.3, 55.3, 11.4, and 6.9 yr, respectively. (ii) The other four components are in harmonic relationship with f_2 and f_5 (Table 1). (iii) The ratio $f_5/f_2 \approx 4.845\,304$ can be considered as an irrational number, suggesting that f_2 and f_5 are two independent frequencies. Consequently, f_1, f_3, f_4, and f_6 are assumed to be harmonic components generated by the nonlinear interaction between f_2 and f_5. (iv) The independent periods L_2 and L_5 suggest connections to a well-known oceanic oscillation and to solar activity, respectively. The period L_5 coincides with solar activity, whereas L_2 is a period close to the cycle of the PDO that characterizes the variability of the North Pacific sea surface temperature on decadal time scales, with a large period band from 50 to 70 yr (Minobe 1999; Wu and Liu 2003).

To investigate how these two fundamental frequencies have influenced the precipitation in the southwestern United States during the past 120 years, the filtered signals (black line) and the respective negative values (red line) are illustrated in Fig. 5. (i) The amplitudes of these filtered signals always change with time, which suggests that the energy of the PDO and the cycle of solar activity acting on the precipitation vary with time. (ii) The amplitude of the filtered signals of solar activity is larger than the PDO. Therefore, solar activity has exerted a greater influence than the PDO on the precipitation in the southwestern United States over the past 120 years. (iii) In general, the slopes (Fig. 5a) of the green ($k_1 = 8.12 \times 10^{-5}$) and purple lines ($k_3 = -1.66 \times 10^{-4}$) are larger than the slope of the smooth blue line ($k_2 = 2.43 \times 10^{-5}$). This indicates that the amplitude S2 gradually increases from 1920 to 1950, remains steady from 1950 to 1980, and decreases remarkably after 1980. Hence, under the influence of the PDO, the precipitation increased from 1920 to 1950, remained unchanged or slightly increased until 1980, and rapidly decreased after the 1980s. (iv) Under the influence of the cycle of solar activity (Fig. 5b), the precipitation in the southwestern United States increased from the 1900s, then decreased substantially after the 1940s. It was not until 1964 that precipitation increased until it dropped again after the 1990s.

Further insight into the causal relationship between precipitation and its driving forces is obtained from the

TABLE 1. Period and frequency of the driving force and relationship between each spectral band.

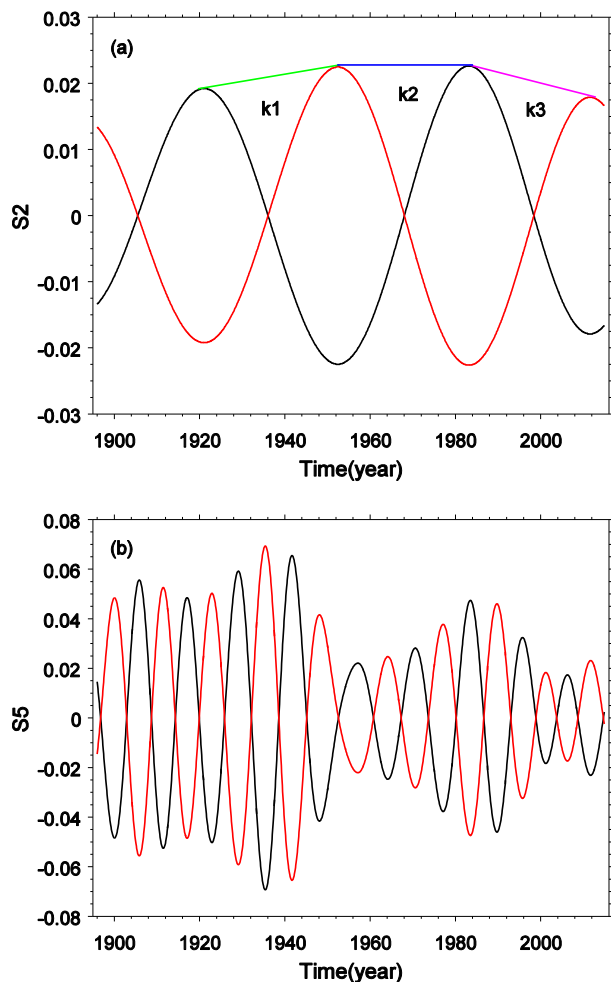| Spectrum	Band	Period (yr)	Frequency (yr^{-1})	Relationship
S1	65.9 and higher	$L_1 = 85.3$	$f_1 = 0.0117$	$6f_1 \approx f_5 - f_2(0.0006)$
S2	42.7–65.8	$L_2 = 55.3$	$f_2 = 0.0181$	Basic frequency
S3	23.3–42.6	$L_3 = 35.9$	$f_3 = 0.0279$	$5f_3 \approx 2(f_5 - f_2)(0.0003)$
S4	16.5–23.2	$L_4 = 18$	$f_4 = 0.0556$	$5f_4 \approx 4(f_5 - f_2)(0.0004)$
S5	9.8–16.4	$L_5 = 11.4$	$f_5 = 0.0877$	Basic frequency
S6	0–9.7	$L_6 = 6.9$	$f_6 = 0.1449$	$f_6 \approx 8f_2(0.0001)$

FIG. 5. Bandpass filters for the reconstruction of the driving force extracted from the monthly mean precipitation anomaly in the southwestern United States: (a) S2 and (b) S5. The black (red) line is the original (negative) value of the filtered signals.

5-yr moving average of the monthly mean precipitation anomaly time series (black line in Fig. 2a). (i) The major droughts in the southwestern United States were in the early 1900s, from the 1950s to the 1970s, and at the beginning of the twenty-first century. (ii) Comparing the drought trend with the above 2 degrees of freedom in the driving forces, the droughts in the 1900s and at the beginning of the twenty-first century were affected by both the PDO and solar activity. However, the PDO had a weak relationship with the droughts occurring from the 1950s to the 1970s, which were mainly affected by solar activity.

4. Discussion and conclusions

SFA was used to extract the driving forces behind the monthly precipitation anomaly time series in the southwestern United States, and their scale structure was interpreted based on wavelet analysis. The following results were obtained: (i) The driving force consists of six main spectral bands; four of them pass the 95% confidence level and correspond to periods of 6.9, 11.4, 55.3, and 85.3 yr. (ii) Further analysis shows that there are only 2 degrees of freedom, which represent the cycle of solar activity and the PDO. The amplitudes of the filtered signals of the two fundamental frequencies change with time, which further indicates that the energy of both forces acting on precipitation varies over time. (iii) The solar activity exerted a greater influence over the precipitation in the southwestern United States than the PDO over the past 120 years. (iv) The droughts in the 1900s and at the beginning of the twenty-first century were affected by both the PDO and solar activity. However, the droughts occurring from the 1950s to the 1970s were mainly affected by solar activity.

In general, SFA provides another approach to investigate and solve the problem of driving forces in the climate system and avoids discrepancies in the understanding of physical processes among scientists. The method is completely different from climate models but functions in parallel with them. Therefore, research on driving forces extracted from time series may have broad applications. Finally, the advantage of the SFA analysis is that it avoids disputes about model uncertainty, although its disadvantage is that it does not provide the underlying physical mechanism. Therefore, more climate model experiments are required to understand the physical mechanisms on how the cycle of solar activity and the PDO affect the precipitation variability in the southwestern United States.

REFERENCES

Casdagli, M. C., 1997: Recurrence plots revisited. *Physica D*, **108**, 12–44, doi:10.1016/S0167-2789(97)82003-9.

Chylek, P., M. K. Dubey, G. Lesins, J. Li, and N. Hengartner, 2014: Imprint of the Atlantic multi-decadal oscillation and Pacific decadal oscillation on southwestern US climate: Past,

present, and future. *Climate Dyn.*, **43**, 119–129, doi:10.1007/s00382-013-1933-3.

Cook, B. I., E. R. Cook, K. J. Anchukatis, R. Seager, and R. L. Miller, 2011: Forced and unforced variability of twentieth century North American droughts and pluvials. *Climate Dyn.*, **37**, 1097–1110, doi:10.1007/s00382-010-0897-9.

——, R. Seager, R. L. Miller, and J. A. Mason, 2013: Intensification of North American megadroughts through surface and dust aerosol forcing. *J. Climate*, **26**, 4414–4430, doi:10.1175/JCLI-D-12-00022.1.

——, ——, and J. E. Smerdon, 2014: The worst North American drought year of the last millennium: 1934. *Geophys. Res. Lett.*, **41**, 7298–7305, doi:10.1002/2014GL061661.

——, E. R. Cook, J. E. Smerdon, R. Seager, A. P. Williams, S. Coats, D. W. Stahle, and J. Villanueva Díaz, 2016: North American megadroughts in the Common Era: Reconstructions and simulations. *Wiley Interdiscip. Rev.: Climate Change*, **7**, 411–432, doi:10.1002/wcc.394.

Cook, E. R., D. M. Meko, D. W. Stahle, and M. K. Cleaveland, 1999: Drought reconstructions for the continental United States. *J. Climate*, **12**, 1145–1162, doi:10.1175/1520-0442(1999)012<1145:DRFTCU>2.0.CO;2.

——, C. A. Woodhouse, C. M. Eakin, D. M. Meko, and D. W. Stahle, 2004: Long-term aridity changes in the western United States. *Science*, **306**, 1015–1018, doi:10.1126/science.1102586.

——, R. Seager, M. A. Cane, and D. W. Stahle, 2007: North American drought: Reconstructions, causes, and consequences. *Earth-Sci. Rev.*, **81**, 93–134, doi:10.1016/j.earscirev.2006.12.002.

——, ——, R. R. Heim, R. S. Vose, C. Herweijer, and C. Woodhouse, 2010: Megadroughts in North America: Placing IPCC projections of hydroclimatic change in a long-term palaeoclimate context. *J. Quat. Sci.*, **25**, 48–61, doi:10.1002/jqs.1303.

Curtis, S., 2008: The Atlantic multidecadal oscillation and extreme daily precipitation over the US and Mexico during the hurricane season. *Climate Dyn.*, **30**, 343–351, doi:10.1007/s00382-007-0295-0.

Douglas, A. V., and P. J. Englehart, 1981: On a statistical relationship between autumn rainfall in the central equatorial Pacific and subsequent winter precipitation in Florida. *Mon. Wea. Rev.*, **109**, 2377–2382, doi:10.1175/1520-0493(1981)109<2377:OASRBA>2.0.CO;2.

Eckmann, J. P., S. O. Kamphorst, and D. Ruelle, 1987: Recurrence plots of dynamical systems. *Europhys. Lett.*, **4**, 973, doi:10.1209/0295-5075/4/9/004.

Enfield, D. B., A. M. Mestas-Nuñez, and P. J. Trimble, 2001: The Atlantic multidecadal oscillation and its relation to rainfall and river flows in the continental U.S. *Geophys. Res. Lett.*, **28**, 2077–2080, doi:10.1029/2000GL012745.

Fawcett, P. J., and Coauthors, 2011: Extended megadroughts in the southwestern United States during Pleistocene interglacials. *Nature*, **470**, 518–521, doi:10.1038/nature09839.

Feng, S., Q. Hu, and R. J. Oglesby, 2011: Influence of Atlantic sea surface temperatures on persistent drought in North America. *Climate Dyn.*, **37**, 569–586, doi:10.1007/s00382-010-0835-x.

Gershunov, A., and T. P. Barnett, 1998: Interdecadal modulation of ENSO teleconnections. *Bull. Amer. Meteor. Soc.*, **79**, 2715–2725, doi:10.1175/1520-0477(1998)079<2715:IMOET>2.0.CO;2.

Gollub, J. P., and S. V. Benson, 1980: Many routes to turbulent convection. *J. Fluid Mech.*, **100**, 449–470, doi:10.1017/S0022112080001243.

Kiladis, G. N., and H. F. Diaz, 1989: Global climatic anomalies associated with extremes in the Southern Oscillation. *J. Climate*, **2**, 1069–1090, doi:10.1175/1520-0442(1989)002<1069:GCAAWE>2.0.CO;2.

Konen, W., 2009: On the numeric stability of the SFA implementation sfa-tk. arXiv.org, 12 pp. [Available online at https://arxiv.org/pdf/0912.1064.pdf.]

Mantua, N. J., S. R. Hare, Y. Zhang, J. M. Wallace, and R. C. Francis, 1997: A Pacific interdecadal climate oscillation with impacts on salmon production. *Bull. Amer. Meteor. Soc.*, **78**, 1069–1079, doi:10.1175/1520-0477(1997)078<1069:APICOW>2.0.CO;2.

McCabe, G. J., M. A. Palecki, and J. L. Betancourt, 2004: Pacific and Atlantic Ocean influences on multidecadal drought frequency in the United States. *Proc. Natl. Acad. Sci. USA*, **101**, 4136–4141, doi:10.1073/pnas.0306738101.

Minobe, S., 1999: Resonance in bidecadal and pentadecadal climate oscillations over the North Pacific: Role in climatic regime shifts. *Geophys. Res. Lett.*, **26**, 855–858, doi:10.1029/1999GL900119.

Oglesby, R., S. Feng, Q. Hu, and C. Rowe, 2012: The role of the Atlantic multidecadal oscillation on medieval drought in North America: Synthesizing results from proxy data and climate models. *Global Planet. Change*, **84–85**, 56–65, doi:10.1016/j.gloplacha.2011.07.005.

Touchan, R., C. A. Woodhouse, D. M. Meko, and C. Allen, 2011: Millennial precipitation reconstruction for the Jemez Mountains, New Mexico, reveals changing drought signal. *Int. J. Climatol.*, **31**, 896–906, doi:10.1002/joc.2117.

Verdes, P. F., P. M. Granitto, H. D. Navone, and H. A. Ceccatto, 2001: Nonstationary time-series analysis: Accurate reconstruction of driving forces. *Phys. Rev. Lett.*, **87**, 124101, doi:10.1103/PhysRevLett.87.124101.

Wang, G., P. Yang, and X. Zhou, 2016: Extracting the driving force from ozone data using slow feature analysis. *Theor. Appl. Climatol.*, **124**, 985–989, doi:10.1007/s00704-015-1475-1.

Wiskott, L., 2003: Estimating driving forces of nonstationary time series with slow feature analysis. arXiv.org, 8 pp. [Available online at https://arxiv.org/pdf/cond-mat/0312317.pdf.]

Woodhouse, C. A., D. M. Meko, G. M. MacDonald, D. W. Stahle, and E. R. Cook, 2010: A 1,200-year perspective of 21st century drought in southwestern North America. *Proc. Natl. Acad. Sci. USA*, **107**, 21 283–21 288, doi:10.1073/pnas.0911197107.

Wu, L., and Z. Liu, 2003: Decadal variability in the North Pacific: The eastern North Pacific mode. *J. Climate*, **16**, 3111–3131, doi:10.1175/1520-0442(2003)016<3111:DVITNP>2.0.CO;2.

Yang, P., G. Wang, F. Zhang, and X. Zhou, 2016: Causality of global warming seen from observations: A scale analysis of driving force of the surface air temperature time series in the Northern Hemisphere. *Climate Dyn.*, **46**, 3197–3204, doi:10.1007/s00382-015-2761-4.

Zhong, W. Y., and P. C. Yang, 1986: The transition of a multidimensional Lorenz system. *Adv. Atmos. Sci.*, **3**, 289–301, doi:10.1007/BF02678650.